# Radiometric temperature reading of a hot ellipsoidal object inside the oral cavity by a shielded microwave antenna put flush to the cheek

**Øystein Klemetsen[1], Svein Jacobsen[1] and Yngve Birkelund[1]**

[1] Department of Physics and Technology, Faculty of Science, University of Tromsø, N-9037 Tromsø, Norway

E-mail: oystein.klemetsen@uit.no, svein.jacobsen@uit.no, yngve.birkelund@uit.no

**Abstract.** A new scheme for detection of vesicoureteral reflux (VUR) in children has recently been proposed in the literature. The idea is to warm bladder urine via microwave exposure to at least fever temperatures, and observe potential urine reflux from the bladder back to the kidneys by medical radiometry. As a preliminary step towards realization of this detection device, we present non invasive temperature monitoring by use of microwave radiometry in adults to observe temperature dynamics *in vivo* of a water filled balloon placed within the oral cavity. The relevance of the approach with respect to detection of VUR in children is motivated by comparing the oral cavity and cheek tissue with axial CT images of young children in the bladder region. Both anatomical locations reveal a triple-layered tissue structure consisting of skin-fat-muscle with a total thickness of about 8-10 mm. In order to mimic variations in urine temperature, the target balloon was flushed with water coupled to a heat exchanger, that was moved between waterbaths of different temperature, to induce measurable temperature gradients.

The applied radiometer has a center frequency of 3.5 GHz and provides a sensitivity (accuracy) of 0.03 $^o$C for a data acquisition time of 2 secs. Three different scenarios were tested and included observation through the cheek tissue with and without an intervening water bolus compartment present. In all cases, radiometric readings observed over a time span of 900 secs were shown to be highly correlated (R$\sim$0.93) with *in situ* temperatures obtained by fiberoptic probes.

## 1. Introduction

For several decades, scientists have been investigating implementation of microwave technology through the use of non-ionizing electromagnetic waves to read *in vivo* temperatures inside the human body (Enander and Larson 1974, Barrett and Meyers 1975, Leroy *et al.* 1998). It is well known that microwave radiometry (Mizushina *et al.* 1995, Stec *et al.* 2004) and infrared techniques (Kennedy *et al.* 2009, Jiang *et al.* 2011) can be applied for non-invasive temperature measurements of superficial tissue. These methods are passive and thus completely harmless as opposed to active methods, including computer tomography (CT) imaging and ultrasonic techniques, that stimulate the body with an excitation signal. Active methods such as ionizing X-rays can in some situations even induce cancer (Guyton and Hall 2000). Standing for 14% of the total annular exposure worldwide, Berrington de Gonzáles and Darby (2004) found that between 0.6% to 3% of the cumulative risk of cancer (to the age of 75) in 15 developed countries can be attributed to diagnostic X-rays.

Microwave radiometry is a well established technique for remote sensing applications of most importance being earth and space observation. In these setups, the electromagnetic waves carrying information can travel without loss over vast distances in air and vacuum providing accurate temperature characterization of radiating objects (Bennett *et al.* 2003, Kerr *et al.* 2001). However, for human body applications, like cancer detection and monitoring of temperature during microwave hyperthermia, the dielectric properties vary strongly with tissue composition and hence spatial heterogeneities make precise interpretation of the measured thermal radiation challenging (Lazebnik *et al.* 2007). Human tissue, including fat and muscle tissue, is lossy with the consequence of limited sensing depth, which further limits the applicability of this observation technique to superficial scenarios. Despite these limitations, microwave radiometry has the potential to be an inexpensive, safe, and non-invasive method for dedicated medical applications (Jacobsen and Stauffer 2003), given that instrumentation (antenna and system hardware) is optimized in each case.

Vesicoureteral reflux (VUR) is a pediatric urinary tract disorder that allows flow of urine from the bladder back up into the ureters and possibly into the kidney. Primary VUR occurs when a child is born with an impaired valve for blocking the urine to reflux from bladder to ureters. Secondary VUR can occur when there is a blockage that hinders normal urine flow. For both situations, infection is the most common symptom of this disease, but secondary VUR infections may also be the direct cause of the urine reflux. Imaging techniques such as e.g. ultrasound may be used to diagnose certain bladder and kidney abnormalities, but can not reveal important urethra dysfunction. Functional imaging techniques, including voiding cystourethrography, require a catheter into the bladder and ionizing radiation (Conway *et al.* 1972, Paltiel *et al.* 1992). These techniques are invasive and should preferably be avoided especially in children.

A new non-invasive modality for primary VUR detection was conceptually introduced by Snow and Taylor (2010). The method is based on heating of the pediatric

bladder above normal body temperature and using microwave radiometry to monitor induced temperature rise in the kidney if a urine reflux occurs. Preliminary results using animal experiments are promising (Snow *et al.* 2011), and data is also encouraging for initial human trials (B. Snow, University of Utah, Salt Lake City, UT USA, private communication). The method has also been evaluated through numerical calculations (Arunachalam *et al.* 2010) and phantom experiments (Arunachalam *et al.* 2011). Common to all this studies is the use of a well established heating device, the so called dual concentric conductor (DCC) antenna, originally developed to treat large area chest wall disease by superficial hyperthermia (Stauffer *et al.* 2010). The novel VUR detecting principle, based on radiometry and applying temperature as a contrast agent, comprises a two steps sequential procedure: i) Heating of the *bladder* using microwaves where the heating process is quality assured with microwave radiometry, ii) detection of heated urine reflux from the *bladder* back into the kidney by radiometric temperature probing of the *kidney*.

In this paper, we solely focus on the first step in the scheme to monitor bladder temperature during heating by means of a low cost, miniaturized, single-band, microwave radiometer. We present dynamic responses of monitored thermal radiation through the cheek muscle and show *in vivo* results using a hot object inside the oral cavity to imitate the observation scenario of a heated bladder.

The remainder of this paper is organized as follows. Section 2 describes the anatomy of the oral cavity and the pediatric bladder as well as methods for acquiring and processing of radiometric data and complementary thermometry. A detailed description of the experimental setup (antenna, radiometer, thermometry, and pumping device) is also given. In addition, supporting numerical simulations of the radiometric setup are described for both a relevant bladder model and the oral cavity model mimicking a pediatric bladder. Section 3 outlines the results and section 4 discusses the findings of the study. Conclusions are given in section 5.

## 2. Methodology

This section gives a description of the different human anatomies involved in the study. Hardware (radiometer and thermometry) and the experimental model as well as supporting numerical models are also described in detail.

### *2.1. Anatomy of cheek and oral cavity*

Looking at the coronal cut plane of the human head, the soft tissues of the human cheeks basically consist of muscle and fat (see figure 1). In humans, muscles are layered and involved in action of expressions and smiles (Shiffman 2010). The cheek is the widest skin surface of the face, is fleshy in humans and covered externally by hairy skin. The skin of the human face has a more abundant blood supply compared with other areas of the body (Semer and Adler-Lavan 2001).

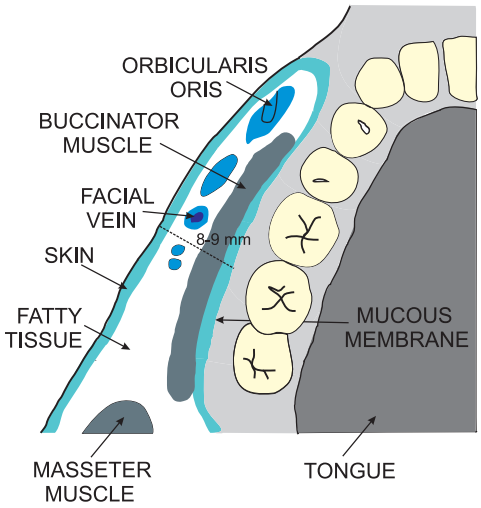


Figure 1: Schematic axial cut of the oral cavity.

Inside of the cheek, forming an interface towards the oral cavity, is the mucous membrane which provides lubrications and protects the oral cavity from infections. The buccinator muscle of the cheeks forms a large part of the lateral wall of the mouth. Buccinator is innervated by the deep buccal branches of the facial nerve and is supplied with blood by the maxillary and facial arteries (Netter 1997, Sherwood 2001).

### *2.2. Anatomy of pediatric bladder*

The placement of the bladder is within the abdomen, underneath skin and fat layers. The urinary bladder is a musculomembranous sac which acts as a reservoir for urine prior to its elimination from the body. Bladder size and position vary according to the amount of fluid it contains (Guyton and Hall 2000). Urine from the kidney is transported by the ureter which has ureter orifices inside and in the lower part of the bladder. There is an urethral sphincter located in the lower part of the bladder that controls flushing of urine from the body through the urethra.

In a newborn child, the internal urethral orifice is at the level of the upper border of the symphysis pubis. The bladder is thus located higher up in infants compared to adults. The inside wall of the bladder has a mucosa membrane whereas the outside is part of peritoneum. The bladder is formed within the body by the detrusor muscle and is layered from outer to inner with circular and longitudinal muscle fibers with sub-mucous coating and transitional epithelium as the inner layer (Gray 1942).

Hiraoka *et al* (1995) estimated the bladder volume of children using ultrasonography. For young children (a few months old) the median bladder volume was about 20 mL. The same technique used on larger children showed a mean volume of 84 mL. Figure 2 shows an axial CT scan of a 3 years old child. Assuming that the third out-of-plane dimension is about 45 mm, the volume is estimated to 60 mL. Observe similarities with the oral cavity in terms of skin, fatty tissue, and muscle layers.

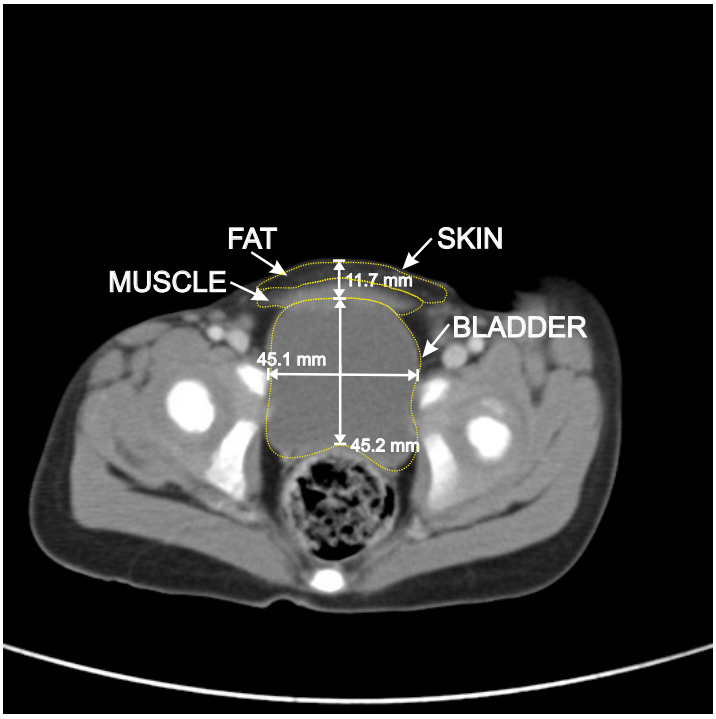


Figure 2: Axial CT scan of 3 years old child with segmentation of intervening tissue and bladder.

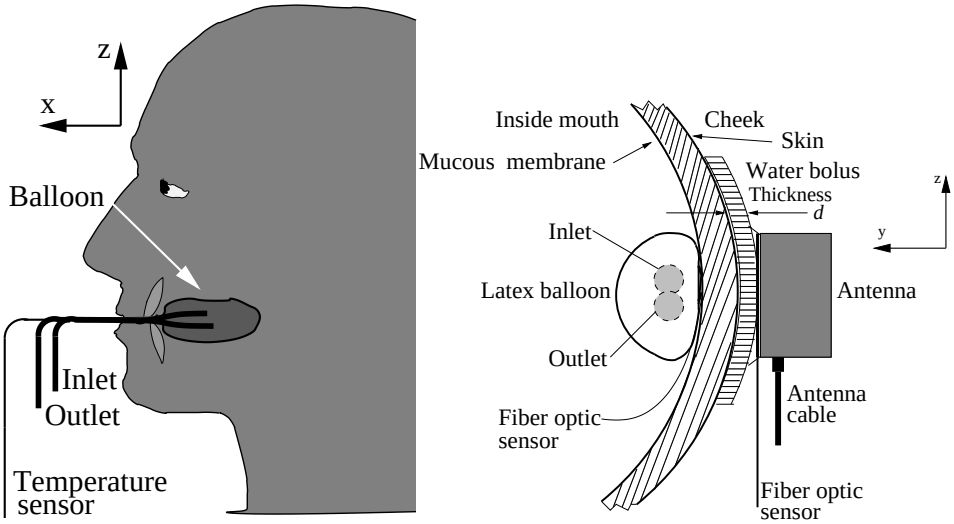


(a) Sagittal plane. (b) Coronal plane.

Figure 3: Experimental setup for dynamic radiometric measurements. (a) Sagittal plane view of radiometric setup including latex balloon inside the oral cavity with inlet and outlet tubes, (b) schematic coronal plane view of oral cavity and antenna put flush to a water bolus of thickness $d$.

### *2.3. Experimental setup details*

The main idea of the *in vivo* setup is to use a balloon with circulated water inside the human oral cavity and an antenna on the outside cheek to observe thermal radiation (see

overview in figure 3a) and details in figure 3b). In the experiment, parts and materials were chosen to avoid damage to the mucous membrane and infections in the oral cavity. More important, the setup renders the possibility of observing thermal objects *in vivo*, through an intervening layer of fat and muscle, without surgical intervention. The target balloon is made of one finger from a thin sterile latex glove. The inlet and outlet of the balloon are constructed from plastic pipes moulded with silicon inside an outer part of a sterile plastic syringe as shown in figure 4. The diameter of the syringe part is $D = 24$ mm, whereas length and width of the target are dependent on the water filled volume of the balloon. If we assume an ellipsoidal shape with dimensions as given in figure 4, the volume of the target is $V = 38$ mL.

The closed loop circulating water system is made from flexible tubes with a diameter of 10 mm, a latex balloon, two waterbaths (Grant VF), a peristaltic pump (Heidolph PD5106), a custom made air trap, and a helical Cu 5/16" heat exchanger (see figure 5). Two water baths of different temperatures $T_c$ and $T_h$ (cold and hot, respectively) are used to induce a temperature step $\Delta T_{c\to h}$ in the balloon, by physically moving the heat exchanger between the water baths. In figure 5, all *in situ* temperatures are measured with fiberoptic probes (IPITEK LT-X5) known only marginally to interfere with the microwave field (Arunachalam *et al.* 2008).

The applied elliptical antenna (Jacobsen and Birkelund 2010, Brelum 2010) for observing thermal radiation is shielded by cavity backing to avoid electromagnetic interference (EMI) from other competing sources. The antenna is made from a Rogers RO4350B substrate of 1.524 mm thickness and fed with a Radiall coaxial cable of type R286301072. The dimensions of the antenna are a frontal square of $40\times40$ mm$^2$ and a nearly cubic backing of 32 mm height. The cavity shield and flanges are soldered together with 0.7 mm copper plate (see figure 6) and the cavity backing is filled with air. Cavity backing is known to limit the bandwidth of microwave antennas due to standing waves. However, since the front side is designed to match a lossy medium, the backward radiation to air is virtually negligible both with and without the shielding cavity present.

In the proposed VUR detection system described by Snow and Taylor (2010), the

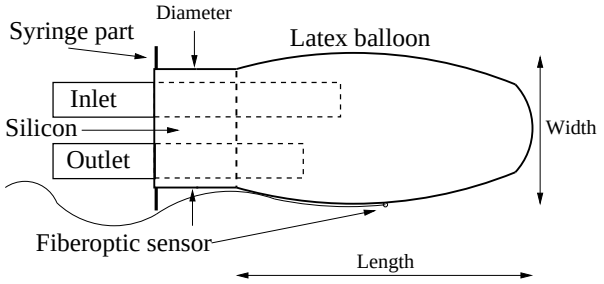


Figure 4: Design details of balloon. The diameter of the syringe part is 24 mm. Length and width of balloon is typically 86 mm and 29 mm, respectively.

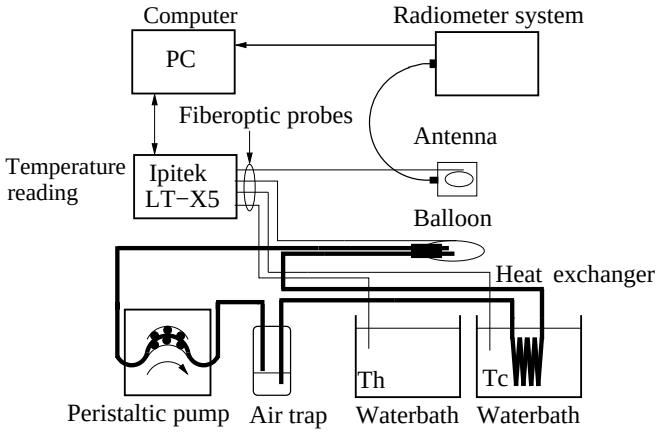


Figure 5: Main components of experimental setup. $T_h$ and $T_c$ are hot and cold water bath temperatures, respectively.

urine temperature inside the bladder is raised to 40-45$^o$C applying an external 915 MHz microwave hyperthermia device (Stauffer *et al.* 2010). When heating the bladder to such high temperatures, the skin temperature has to be controlled with the use of a water circulated bolus to prevent blisters from the high-energetic nearfields. Using radiometry to monitor temperature changes within the bladder, the antenna should preferably be put flush to the skin to maximize the radiometric response. However, due to limited space on the skin in the proximity of the bladder, the radiometer antenna could either be located on top of the bolus near the heating antenna, or put flush to the skin after removal of the heating device. Nevertheless, both scenarios have been considered in this study as it is presently not known which solution will be optimal.

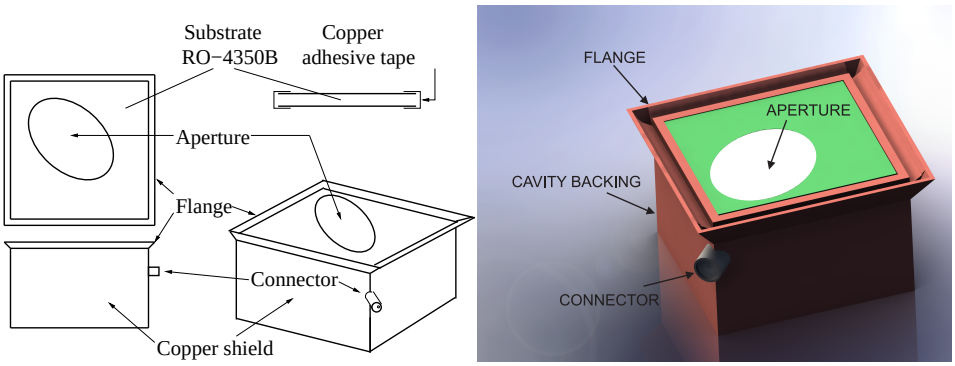


(a) Design details. (b) 3-D view of CAD drawing.

Figure 6: Design details and perspective view of shielded elliptical antenna.

### *2.4. Radiometer system*

A microwave radiometric system is an instrument that can read non invasive temperatures in the human body by measuring noise power emitted by any load material above absolute zero temperature (Land 1983, Leroy *et al.* 1987, Carr 1989, Mizushina *et al.* 1995, Leroy *et al.* 1998). Often, a microwave radiometer uses a specific, but relatively broad, frequency band to obtain a readable noise level. The thermal signal is then amplified to a power range between -60 dBm to -25 dBm in order to be detected by a square law detector (Pozar 2004).

Blackbody spectral radiance vs frequency at temperature $T$ is given by Planck's law:

$$I(f,T) = \frac{2hf^3}{c^2}\frac{1}{e^{\frac{hf}{kT}}-1}, \tag{1}$$

where $f$ is the frequency in Hz, $T$ is temperature in Kelvin, $k$ is Boltzmann's constant, $h$ is Planck's constant and $c$ is speed of light. The total radiance emitted in a frequency band can be obtained by integrating $I(f,T)$ over the frequency band $\Delta f = f_2 - f_1$:

$$\int_{f_1}^{f_2} I(f,T)\mathrm{d}f. \tag{2}$$

For frequencies in the microwave region and body temperatures around 310 K, Planck's law can be approximated by Rayleigh-Jean's law (Reeves *et al.* 1975):

$$I(f,T) = \frac{2kTf^2}{c^2} \tag{3}$$

from which the noise power $P$ can be written as (Ulaby *et al.* 1981):

$$P = kT\Delta f. \tag{4}$$

The observed radiometric temperature can be modeled by the following equation (Jacobsen and Klemetsen 2008):

$$T_B = (1-\rho)\int_V W(\vec{r})\,T(\vec{r})\,\mathrm{d}V + (1-\rho)\,T_{EMI} + T_e \tag{5}$$

where $T_B$ is the brightness temperature, $\rho$ is the power reflection coefficient between antenna and load, $W(\vec{r})$ is the radiometric weighting function, $T(\vec{r})$ is the spatial

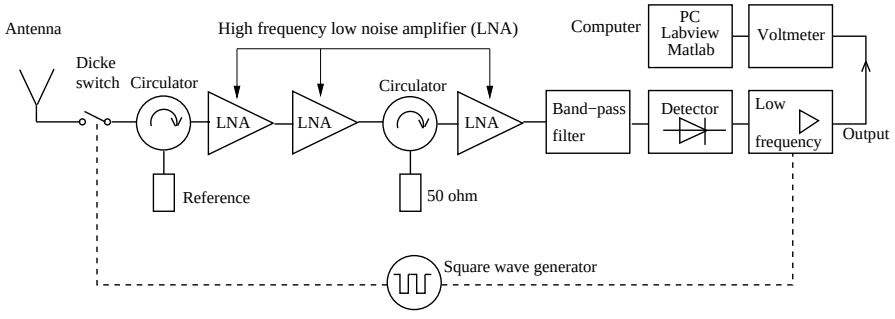


Figure 7: Schematic block diagram of the radiometer.

Table 1: Radiometer system parameters.

| Parameter | Notation | Value |
|---|---|---|
| Operation center frequency | $f$ | 3.5 GHz |
| Bandwidth of front-end (-3 dB) | $\Delta f$ | 720 MHz |
| Integration time in post processing | $\tau$ | 2 s |
| Sensitivity with 50 Ω load and $\tau$=2 s | $\sigma$ | 0.03 K |
| Sensitivity with antenna load and $\tau$=2 s | $\sigma$ | 0.11 K |
| Reference temperature | $T_{ref}$ | 290 K |
| Sampling frequency | $f_s$ | 457.8 Hz |

temperature distribution of the object at the position $\vec{r}$, $T_{EMI}$ is the electromagnetic interference, and $T_e$ is the equivalent noise temperature in the radiometer. The radiometric weighting function can be written as:

$$W(\vec{r}) = \frac{P_d(\vec{r})}{\int_V P_d(\vec{r})\mathrm{d}V}. \tag{6}$$

Here, $P_d$ is the power deposition density given by: $P_d = (\sigma_m(\vec{r})/2)|\vec{E}(\vec{r})|^2$ where $\vec{E}$ and $\sigma_m$ is the electric field and conductivity, respectively, within the medium. The weighting function is normalized according to (Reeves *et al.* 1975):

$$\int_V W(r)\mathrm{d}V \equiv 1. \tag{7}$$

If the radiometric system is properly shielded, the $T_{EMI}$ part in (5) can be small enough to be ignored. We can also improve the equivalent noise temperature in the radiometer hardware as described in Jacobsen and Klemetsen (2008) and Klemetsen *et al* (2011). Radiometric data fluctuate randomly like noise. The standard deviation $\sigma$ (equivalent to the system accuracy) of the stochastic fluctuations is a measure of brightness temperature resolution, and can be written as (Ulaby *et al.* 1981):

$$\sigma = \frac{2(T_A + T_e)}{\sqrt{\Delta f \tau}}, \tag{8}$$

where $\Delta f$ is the integration bandwidth, $T_A = T_B$ is the antenna temperature, $\tau$ is the integration time and requiring a balanced mode of $T_A$=$T_{ref}$, the latter parameter being the reference channel temperature (see figure 7).

If the radiometer is calibrated with two known temperatures above and below the operation temperature, the slope is given by:

$$s = \frac{V_{cal,h} - V_{cal,c}}{T_{cal,h} - T_{cal,c}}, \tag{9}$$

where $V_{cal,h}$ and $V_{cal,c}$ are the radiometer output voltages at $T_{cal,h}$ and $T_{cal,c}$, hot and cold known temperatures, respectively. The absolute measured temperature is then

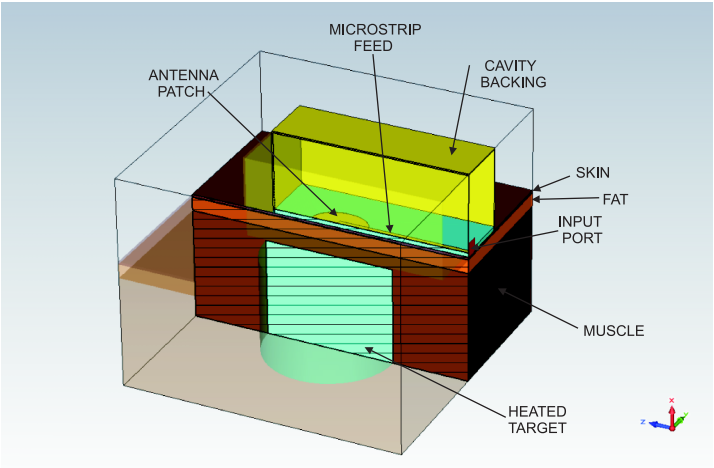


Figure 8: Cutaway view of numerical model

given by (Ulaby *et al.* 1981):

$$T_B = \frac{V}{s} - \left( \frac{V_{cal,c} T_{cal,h} - V_{cal,h} T_{cal,c}}{V_{cal,h} - V_{cal,c}} \right) \tag{10}$$

where $T_B$ is the measured brightness temperature and $V$ is the radiometer output voltage. If the radiometer is calibrated with a 50 Ω load in a waterbath, the measured brightness temperature $T'_B$ of an antenna is given by (Hand *et al.* 2001):

$$T'_B = (1 - \rho)\, T_B \tag{11}$$

where $T'_B \leq T_B$ depending on the power reflection coefficient $\rho$.

The radiometer used in this experiment is an analog Dicke radiometer (Pozar 2004). The front end is implemented using mainly the same components as described in Klemetsen *et al* (2011), but was further improved with use of a circulator of type 3CDMG35-4 from Dorado International† as well as a more sensitive detector of type HMC602LP4 from Hittite‡. A schematic block diagram of the radiometer is depicted in figure 7 and specifications are given in table 1. The output voltage from the radiometer is measured with a digital HP34401 multimeter and the system is controlled by a PC over the GPIB/USB interface, and running a LabView script to give a quick look and disc save of observed data readings. Post-processing of the sampled data is done in Matlab.

### *2.5. Numerical modeling*

Electromagnetic full-wave numerical simulations of both the experimental oral cavity phantom and the bladder geometry were run by the commercial software package CST Microwave Studio§. A common model for both scenarios was adopted and comprise

† http://dorado-intl.com/
‡ http://www.hittite.com/
§ http://www.cst.com/

Table 2: Numerical model parameters.

| | Model | |
|---|---|---|
| Parameter | Bladder | Oral Cavity |
| $d_{skin}$ [mm] | 1 | 1 |
| $d_{fat}$ [mm] | 5 | 5 |
| $d_{muscle}$ [mm] | 5 | 2 |
| target content | urine | water |

a layered structure of skin, fat, muscle, and target (see tables 2 and 3 for details on dimensions and dielectric properties, respectively). A bolus was also included for some of the cases. The target shape was assumed to be cylindrical with height and radius according to the balloon (see figure 4) and bladder (see figure 2) dimensions.

Fig 8 shows a xz-plane cutaway view of the model exported from the software package (no bolus shown). The brightness temperature (equation (5)) was generated numerically by multiplying the 3-D distribution of the weighting function (equation (6)) with the spatial temperature distribution $T(\vec{r})$. Normalization was performed to yield $T_B$=310 K before heating of the system in thermal equilibrium. The target temperature was thereafter raised by 5 K to generate $\Delta T_B$ for the various cases.

Since the depth location of the target is slightly different in the two models, different size parameter values were used to accommodate for any dissimilarities. Also, the dielectric properties of the target were varied as the bladder model was assumed to be filled with urine whereas the oral cavity balloon model contained water.

Table 3: Dielectric properties of some materials @ 3.5 GHz (Gabriel *et al.* 1996).

| Medium | $\epsilon_r$ | $\sigma$ [S/m] |
|---|---|---|
| Muscle | 51.4 | 2.55 |
| Fat | 5.2 | 0.16 |
| Skin | 37.6 | 2.02 |
| Urine | 73.5 | 4.91 |
| Water | 76.0 | 2.90 |

## 3. Results

Below we present the experimental and numerical results obtained in the study.

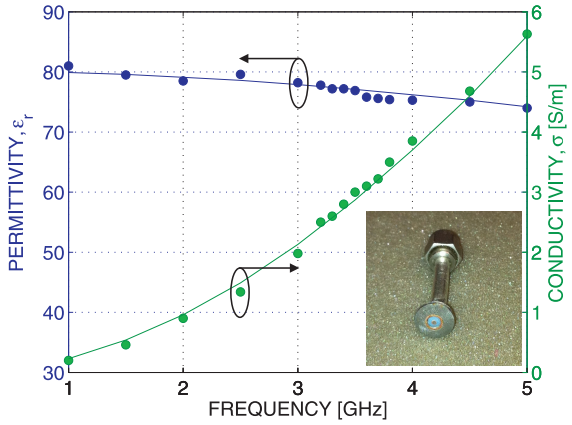


Figure 9: Comparison of probe measured dielectric properties of water (•) and literature values (solid line) (Meissner and Wentz 2004).

### *3.1. Dielectric properties of cheek*

Dielectric properties of the antenna load materials were obtained using an open-ended coaxial line technique originally suggested by Athey *et al* (1982). A 8-mm diameter flange was included at the probe aperture as suggested by Zheng and Smith (1991) to improve the accuracy of the measurements. Moreover, a pointwise estimate of the complex dielectric constant was derived by running a full wave simulation (CST Microwave studio) of the medium-loaded probe and comparing return loss $S_{11}$ with measurements generated by a network analyzer. A Nelder-Mead Simplex procedure was used to minimize the difference $\delta(\hat{\epsilon}_m, \hat{\sigma}_m, f) = (S_{11}^{mod} - S_{11}^{meas})^2$, where permittivity $\hat{\epsilon}_m$ and conductivity $\hat{\sigma}_m$ are to be estimated. Typically, 25-30 iterations were needed to obtain convergence of the Simplex algorithm. To reach accuracy within a few percent when compared to literature data (see figure 9), 1 MVoxels had to be used in the EM model of the probe, resulting in 8-10 h execution time for one data point on a 2.66 GHz quad-core computer.

Figure 9 shows permittivity and conductivity for water in the range from 1 to 5 GHz, and comparisons are made with literature data. Overall, the concordance between model and measurements is satisfactory for both parameters.

The permittivity and conductivity were thereafter measured on the surface of the cheek and mucous membrane in the oral cavity as a function of frequency. No attempts were made to measure the permittivity as a function of position on the cheek. Rather, the "midpoint" of the cheek was selected. This point was defined as the intersection between the vertical line starting at the eye going downwards and the horizontal line in-level with the gap between the upper and lower row of teeth. This is also the point where the antenna was mounted. The obtained results within the radiometric band from 3.2 to 3.8 GHz are shown in figure 10. We observe somewhat higher values for both parameters of the mucous membrane as a direct consequence of more muscle like

tissue close to the surface inside the oral cavity compared to the more fatty tissue on the cheek. Numerical differences of the dielectric parameters derived at the two anatomical sites are consistent, but offset in absolute value, with observations made by Higashi and Ishihara (1990) who obtained $\epsilon_{cheek}$=30, $\sigma_{cheek}$=2.2 S/m and $\epsilon_{muc}$=56, $\sigma_{muc}$=2.7 S/m at 3.5 GHz using a pulse-reflection technique (compare to figure 10). Since physiological factors will vary between individuals, and the sensing volume is dependent on the probe construction, these variations might be expected. Overall the cheek tissue volume can be regarded as slightly heterogeneous consisting of fatty infiltrated muscle tissue.

### *3.2. Antenna matching*

A critical factor when coupling through a layered, lossy medium to observe a heated object at depth, is the ability of the sensing antenna to couple efficiently to the volume under investigation. This can be seen from equation (5), which states that as the reflection coefficient $\rho$ increases, the information content in the thermal signal from the heated object will become small compared to equivalent noise temperature of the radiometer. Hence, a poorly matched antenna will evidently lower the sensitivity of the radiometer. The scattering parameter $S_{11}$ of the antenna was measured by a network analyzer (HP8719D) directly on the human cheek and on water filled boli (put flush to the cheek) of thickness 3 and 7 mm (see figure 11). In the radiometric band, centered at 3.5 GHz, the matching is excellent, especially for the cheek (-20 dB). Also with the intervening boli present, $S_{11}$ <-10 dB throughout the 700 MHz band around 3.5 GHz.

### *3.3. Radiometric balloon response*

In order to test the dynamic step response of the setup, initial testing was conducted with the elliptical antenna put in direct contact with the balloon. Due to thermal gradients in both the latex balloon wall and heat exchanger material, a time delay

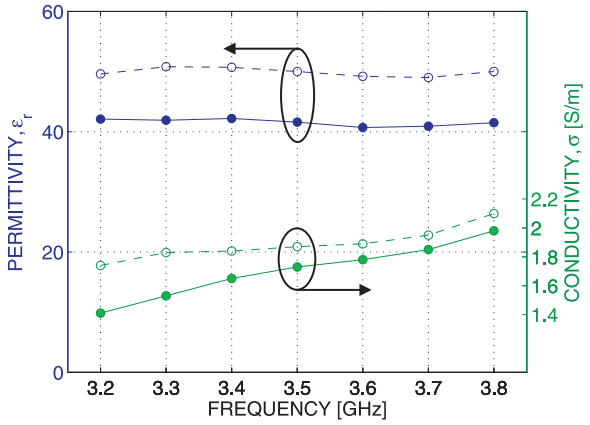


Figure 10: Measured dielectric properties of *in vivo* tissue. (•): cheek and (○): mucous membrane inside oral cavity.

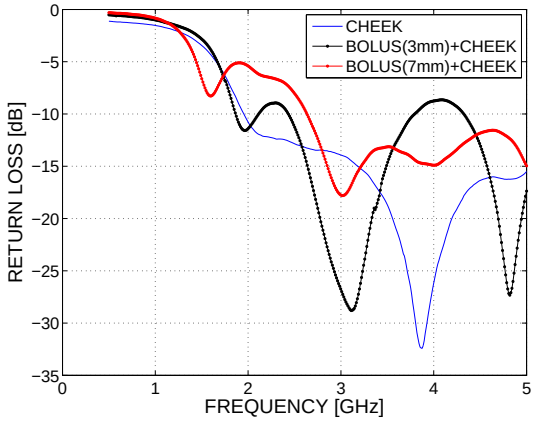


Figure 11: Measured $S_{11}$ of shielded elliptical antenna flush on cheek and through water filled bolus in contact with cheek.

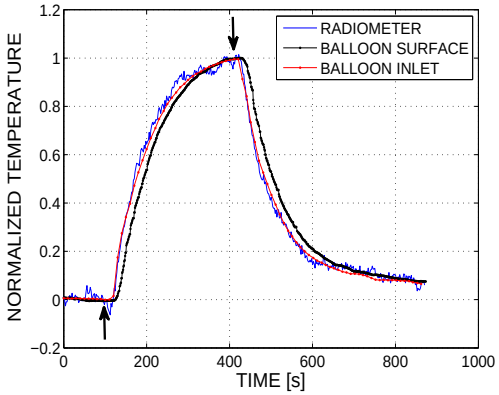


(a) Vertical arrows mark trigger points where the heat exchanger is moved between water baths.

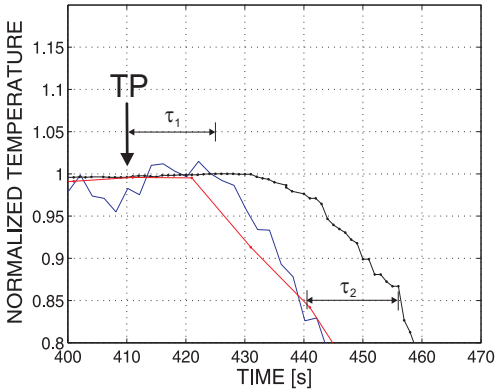


(b) Trigger point TP (vertical arrow) and delay times (horizontal double arrows). $\tau_1$=15 s: time delay between TP and radiometer/balloon inlet. $\tau_2$=17 s: time delay between radiometer/balloon inlet and balloon surface.

Figure 12: Step responses of fiberoptic temperatures (on balloon surface and inside inlet tube) and brightness temperature.

in the temperature step response, relative to the point-in-time movement of the heat exchanger between the water baths, is *a priori* expected. Figure 12 indeed verifies this expectation as shown by the normalized step responses for both brightness temperature and fiberoptic probes. The following characteristics can be induced from the plots. First, there is an approximate $\tau_1$=15 secs time delay between trigger point TP (movement of heat exchanger) and water inlet temperature of the balloon. This can be related to thermal conduction through the heat exchanger wall which consists of 2 mm thick copper with high thermal conductivity (400 W/mK). Second, the water inlet temperature is

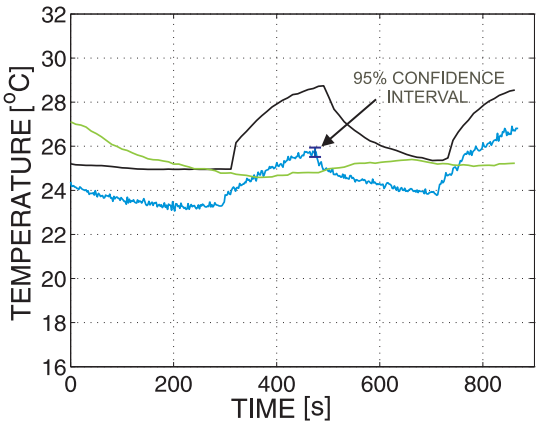


Figure 13: Observed temperatures during radiometric experiment coupling directly to cheek. $T_B$ (blue line), balloon surface (black line), and antenna aperture (green line). $T_h$= 29.2°C, $T_c$= 24.2°C. 95% confidence interval of $T_B$ is 0.44 $^o$C.

synchronized in time with the radiometric readings. As the hot water front enters the balloon, the radiometer immediately responds to the temperature change, since the radiation source emits electromagnetic waves that propagate through the thin latex wall with the speed of light. Third, there is an additional $\tau_2$=17 secs time delay between the radiometric step response and the balloon *outer surface* temperature. This is due to thermal conduction through the balloon wall which is thin (sub-millimeter thickness), but consists of a latex material with low thermal conductivity (0.20 W/mK). As the flow rate is high, the time delay from propagation of the water through the 1 m long tubes can be neglected.

### *3.4. Human in vivo experiments*

Human experiments were conducted with the first author as a volunteer. Initially, the thickness of the cheek was measured to 8-9 mm using a slide caliper (see Figure 1). The volume of the balloon varied somewhat and was estimated for each experiment by measuring the ellipsoid major and minor axes.

An initial experiment was conducted with the antenna put flush to the skin of the cheek (see figure 13). During the data acquisition period, the heat exchanger was moved four times between the waterbaths giving a total of two pulse responses. The target balloon volume was estimated to 38 mL. A temperature difference of only $\Delta T_{c\to h}$=5 $^o$C was used to maintain relevance with respect to realistic microwave heating temperatures that can be expected in the bladder. The blood perfusion within the cheek is relatively high resulting in an overall increase of the antenna aperture temperature in time (green line in figure 13), even though the mucous membrane is loaded by the colder water-flushed balloon. We observe a marked correlation between the brightness temperature $T_B$ and the balloon surface temperature with a similar time delay between the curves as discussed above in section 3.3.

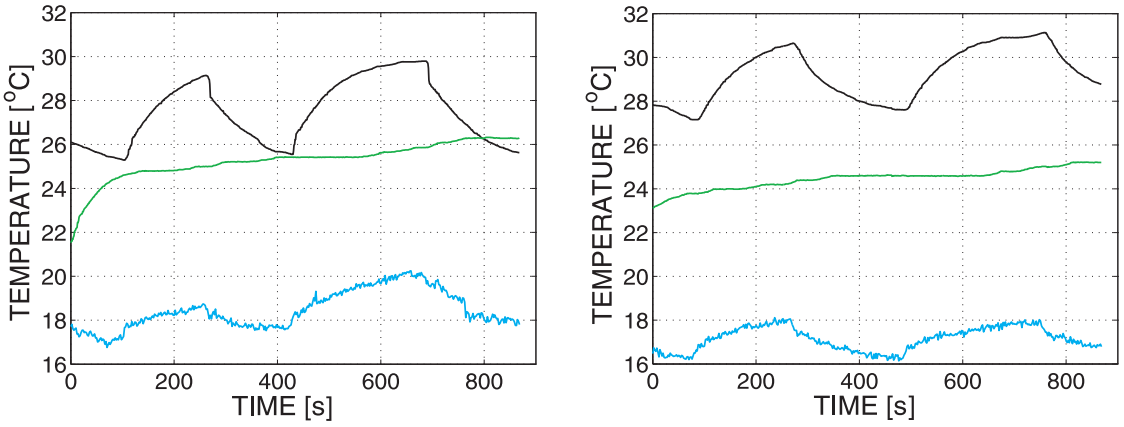


(a) 3 mm thick bolus

(b) 7 mm thick bolus

Figure 14: Same as figure 13, but observing through a water filled bolus. $T_B$ (blue line), balloon surface (black line), and antenna aperture (green line). $T_h$= 29.4°C, $T_c$= 24.5°C.

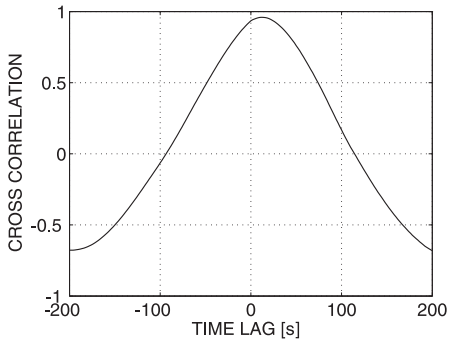


Figure 15: Normalized cross correlation function between radiometric brightness temperature and balloon surface temperature. Maximum correlation coefficient $R$ = 0.96 at time lag $\tau_d$=12 secs.

In figures 14a and 14b, measurements with two different intervening water boli between the antenna and the cheek are depicted. The balloon volume was estimated to be 35 mL for both experiments. Again, we observe the covariation described above, but with smaller amplitude fluctuations of $T_B$ as a direct consequence of the lossy bolus. In order to quantify the temperature covariation, the normalized cross correlation was generated for each case. A representative example is shown in figure 15, from which a maximum correlation coefficient of $R$ = 0.96 occurring at time lag $\tau_d$=12 secs can be estimated. The 12 secs time lag is consistent with the $\tau_1$=15 secs time lag observed in figure 12. Table 4 summarizes the peak-to-peak brightness temperature and maximum correlation coefficient for all three cases.

Table 4: Experimental key parameters.

| 0 mm bolus | | 3 mm bolus | | 7 mm bolus | |
|---|---|---|---|---|---|
| $\Delta T_B{}^a$ | $R^b$ | $\Delta T_B$ | $R$ | $\Delta T_B$ | $R$ |
| 2.2$^o$C | 0.91 | 2.0$^o$C | 0.93 | 1.8$^o$C | 0.96 |

[a] peak-to-peak value
[b] maximum cross correlation

### *3.5. Numerical results*

A crucial factor in radiometric thermometry probing of lossy media is the volumetric dependency of the radiometric weighting function. Figure 16 exemplify this parameter for the oral cavity model. We observe low values of $W$ in the fat layer and higher values in the skin and bolus layer as well as moderate values in the muscle layer. Overall, this can be expected from the respective conductivity values (table 3) although standing wave effects within the thin layers also influence the steady state power distribution pattern. Furthermore, $W(\vec{r})$ decreases exponentially with depth in the heated target. However, due to the large target volume and limited depth location, this radiation is expected to add up significantly in the integral of the brightness temperature $T_B$ (see equation (5)). Following the procedure outlined in Section 2.5, the various excess

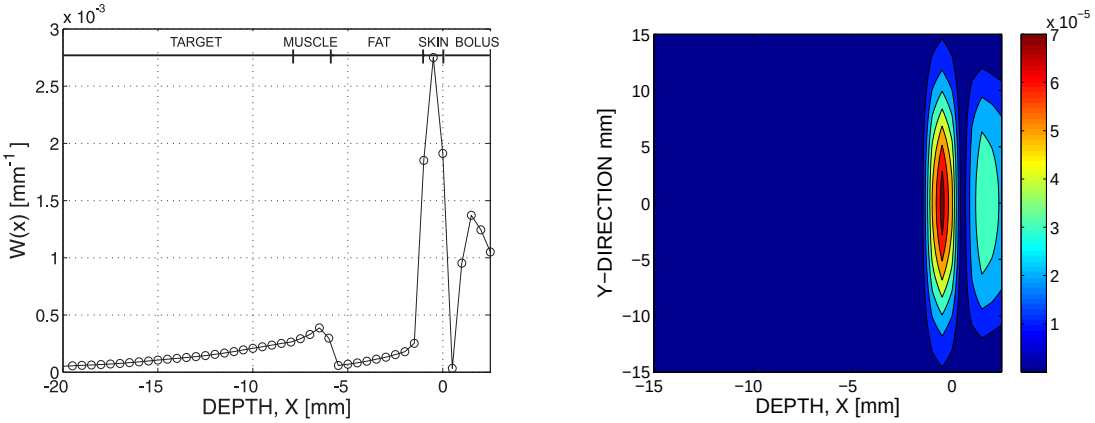


(a) 1-D weighting function against depth x with layers.

(b) 2-D weighting function against depth x and transversal direction y.

Figure 16: Radiometric weighting function for oral cavity model using a 3 mm thick bolus.

brightness temperatures $\Delta T_B$ were generated for comparison to experimental data and to evaluate relevance with respect to the VUR bladder model. The radiometric responses were derived using a 5$^o$ C temperature increase of the target. Table 5 summarizes the results for the various cases. Overall, we observe a marked decrease in $\Delta T_B$ vs increased bolus thickness. Also, the absolute $\Delta T_B$-values are smaller for the bladder model as a

Table 5: Estimated numerical brightness temperature $\Delta T_B$ [$^o$C] response to a 5 $^o$C increase in target temperature.

| | Model | |
|---|---|---|
| Bolus thickness [mm] | Bladder | Oral Cavity |
| 0 | 1.64 | 2.31 |
| 3 | 1.28 | 1.80 |
| 7 | 0.93 | 1.29 |

consequence of a thicker muscle layer, but still markedly above the expected thermal noise level of the hardware instrumentation.

## 4. Discussion

Microwave thermography provides a low-cost, noninvasive, passive, and inherently safe observation technique for inferring temperature distributions within superficial parts of the body. Recently, a microwave-based diagnostic system with a 915 MHz antenna array for non-invasive bladder heating to 40-45$^o$C and a sensitive radiometer for detection of warm urine reflux in kidneys from the bladder, was suggested by Snow and Taylor (2010).

According to Snow *et al* (2011), CT images of children (age 2-5 years) show a distance of about 10 mm from the skin interface to the anterior bladder surface and correspondingly 30 mm to the center of the bladder. A representative CT image depicted in figure 2 displays these distances to be 11.7 mm and 34.3 mm, respectively. The cheek tissue in adults provides much of the same anatomical tissue-layered structure, and can serve as a test bed for this temperature monitoring concept, if combined with a warm object placed inside the oral cavity to mimic the heated bladder.

Nonetheless, there are both structural and observational differences, but also relevant similarities between the oral cavity and the bladder region. First, the total thickness of the intervening layers is slightly thicker (about 1-2 mm) for the bladder compared to the cheek. As mentioned above, the tissue is triple-layered consisting of skin, fat, muscle, and target (bladder or balloon) in both anatomical locations. For the cheek tissue, this was verified by probe measurements, which showed larger values of both permittivity and conductivity at the mucous membrane compared to the outer skin interface that contains more fatty tissue (figure 10). Second, the balloon volume is (of practical reasons) about half the volume (35 mL) of a typical pediatric bladder (75 mL). This directly affects the contribution to the target brightness temperature with a weaker radiometric signal emitted from the smaller water-filled balloon. Third, the fluidic content of the targets is water and urine. At 3.5 GHz, the conductivity of urine is somewhat higher ($\sigma_u$=4.91 S/m (Dietsch *et al.* 2000)) than water ($\sigma_w$=2.9 S/m, see figure 9). From equation (6), it is seen that the weighting function is proportional to

the conductivity, making the urine volume a stronger radiometric source than the water volume. Overall, we conclude that the oral cavity, heated balloon setup poses a similar radiometric challenge as measuring in the bladder region of infants.

Antenna matching is a critical factor in medical radiometry as a low reflection coefficient at the load-antenna interface is imperative to maintain acceptable performance. A shielded elliptical microstrip antenna was used in the reported experiments. The antenna was documented to be well matched to all loading materials including the cheek volume with or without an intervening water filled bolus present. As no Faraday cage was used during the experiments, backward shielding was necessary to avoid interference from competing sources. We stress inclusion of the square flange (see figure 6) as being very important to prevent EMI from entering laterally through the edges of the printed circuit board.

Initially, the antenna was put flush to the balloon to observe the dynamic temperature responses as the heat exchanger was moved between the cold and hot waterbaths. Small, but marked time delays due to heat conduction through both the heat exchanger and balloon walls were observed. These time delays (of about 15 secs) were consistent with *a priori* expectations and were also present in the human experiments. To imitate a heating scenario with a bolus present, the flushing dynamics were also observed through two different boli of 3 mm and 7 mm thicknesses. Table 4 summarizes the radiometric peak-to-peak value and correlation between radiometric and probe measurements for all three cases. We observe a consistent decrease in $\Delta T_B$ as the bolus thickness increases.

Interpretation and comparison of temperature data are important in order to understand the dynamics of the experiments. In the initial experiment, the antenna is put in direct contact with the skin. The aperture temperature decreases in the first part of the experiment before the first temperature step is induced (see figure 13), but increases thereafter slightly in time due to heating by the *in vivo* tissue. For the other two experiments, we initially observe an *increase* of the aperture temperature (see figures 14a and 14b). Here, the antenna is put flush to a colder bolus which again is heated by the warmer cheek. Similarly to the first experiment, the antenna aperture temperature increases monotonously in time due to heating by the *in vivo* tissue. Furthermore, for the temperature probe mounted on the balloon surface inside the oral cavity, the dynamical trends are totally different. From figures 13-14b it is seen that the average temperature of the balloon surface (black line) increases from about 26 $^o$C to 29 $^o$C as the bolus thickness is increased. Hence, since the fiberoptic probe is mounted on the balloon surface with tape, a high temperature is equivalent to a tight physical coupling between the balloon and the hotter mucous membrane, given that the probe temperature displays a weighted average between the tissue temperature and the circulating water. This phenomenon can explain the relatively marginal (about 0.4$^o$C) decrease in peak-to-peak brightness temperature vs bolus thickness. The reduction is smaller than intuitively expected as water produces considerable EM loss at 3.5 GHz. However, tighter physical coupling (as in the bolus experiments) between the mucous

membrane and the balloon will affect the transmission properties of thermal radiation through this interface. A 1% higher EM transmission coefficient at this interface is equivalent to $3^oC$ increase in brightness temperature.

Apart from the peak-to-peak value of the brightness temperature, the average value should also display important information. The absolute mean values of $T_B$ are $24.5^oC$ (0 mm bolus), $19.5^oC$ (3 mm bolus), and $17.5^oC$ (7 mm bolus). As the bolus thickness increases, the balloon target is moved away from the antenna and thus the weighting function becomes more dominated by the material closest to the aperture. Thus, since the bolus water was colder than the balloon water, the brightness temperature mean value should decrease with increasing bolus thickness.

In order to evaluate the radiometric results with respect to absolute target response and measured contrast relative to the noise level of the temperature signal, supporting numerical simulations were also run. The following can be derived by comparing experimental data (table 4) with numerical results in table 5. First, evaluating the numerical models, $\Delta T_B$ was systematically lower (about 0.4-0.7$^o$C) for the bladder model compared to the oral cavity model, but still far above the noise level of $0.11^oC$. Both models displays a systematic decrease in $\Delta T_B$ with increasing bolus thickness. Hence, the responses indicate a clear radiometric similarity between the oral cavity model and the pediatric bladder model, the latter being to some extent more challenging as the muscle layer is expected to be slightly thicker when measuring at the abdomen. Second, the experimental and numerical oral cavity models roughly display the same response of about 2.2-2.3$^o$C (no bolus). For the 7 mm bolus cases, the numerical response decreases with about $1.0^oC$ whereas the corresponding experimental reduction is only $0.4^oC$. A plausible explanation for this discrepancy is a small compression of the bolus when the antenna is mounted onto it during the experiment.

With the intention of using microwave radiometry for quality assurance of the bladder heating process, some kind of inversion scheme is needed to estimate the actual bladder temperature from the measured brightness temperature. Fortunately, *a priori* knowledge about the intervening tissue composition and (if any present) bolus configuration between antenna and target simplifies the problem. According to Jacobsen and Stauffer (2007), errors arising from realistic deviations from base values of dielectric and thermal parameters have only marginal impact on performance of the temperature retrieval scheme. However, pronounced deviations were observed for unknown variations in design model parameters such as bolus thickness and temperature. We emphasize the need to pay particular attention to applicator construction parameters in future clinical implementation of the thermometric method.

Although the radiometric part of the new VUR detection technique is completely passive, the active heating procedure of the bladder involves a risk of producing blisters at the skin interface and overheating the urine. As the target patient group consists of small children, these potential side effects need to be addressed in future work. Nevertheless, in a recent paper by Snow *et al* (2011), pathological evaluation of three pigs (where the urine was heated to 40-44$^o$C) showed that heating could be done without

tissue damage, mainly due to the low power levels (10-20 W) needed to maintain elevated bladder temperatures.

## 5. Conclusions

Vesicoureteral reflux (VUR) is known to induce kidney scarring in children. A new non-invasive VUR detection device, based on microwave heating (915 MHz) of the bladder and radiometric observation of heated refluxed urine, is under development. This study is focused at the potential of radiometrically observing heated urine within the bladder for quality assurance of the warming process. To mimic this scenario, a water-filled balloon was placed inside the oral cavity and the flushing temperature dynamics were observed through the 8-9 mm thick cheek tissue with and without an intervening bolus layer present. In all cases, dynamic radiometric responses were measured and shown to be consistent with *in situ* measured temperature gradients (of only 5 $^{o}$C) obtained from fiberoptic sensors. The proposed diagnostic system has the potential to facilitate non-invasive VUR detection avoiding bladder catheterization, patient sedation, and exposure to ionizing radiation in children.

## Acknowledgments

The authors thank professor Brent Snow, University of Utah, Salt Lake City, UT, USA for providing the CT image used in the paper. Øystein Klemetsen and Yngve Birkelund are grateful for the opportunity of spending the academic year 2009-2010 at Duke University Medical Center in Durham, NC, USA.

## References

Arunachalam K, Maccarini P, De Luca V, Bardati F, Snow B and Stauffer P R 2010 Modelling the detectability of vesicoureteral reflux using microwave radiometry *Physics in Medicine and Biology* **55** 5417–5435

Arunachalam K, Maccarini P, De Luca V, Tognolatti P, Bardati F, Snow B and Stauffer P R 2011 Detection of vesicoureteral reflux using microwave radiometry - system characterization with tissue phantoms *IEEE Trans on Biomedical Engineering* **58** 1629–1636

Arunachalam K, Maccarini P, Juang T, Gaeta C and Stauffer P R 2008 Performance evaluation of a conformal thermal monitoring sheet sensor array for measurement of surface temperature distributions during superficial hyperthermia treatments *International Journal of Hyperthermia* **24** 313–325

Athey T W, Stuchly M A and Stuchly S S 1982 Measurement of radio-frequency permittivity of biological tissues with an open-ended coaxial line. 1. *IEEE Trans on Microwave Theory and Techniques* **30** 82–86

Barrett A H and Meyers P C 1975 Subcutaneous temperatures: A method of noninvasive sensing *Science* **190** 669–671

Bennett C L, Halpern M, Hinshaw G, Jarosik N, Kogut A, Limon M, Meyer S S, Page L, Spergel D N, Tucker G S, Wollack E, Wright E L, Barnes C, Greason M R, Hill R S, Komatsu E, Nolta M R, Odegard N, Peiris H V, Verde L and Weiland J L 2003 First-year wilkinson microwave anisotropy (wmap) observations: Preliminary maps and basic results *Astrophysical Journal Supplement Series* **148** 1–27

Brelum S H 2010 Ultrawideband (UWB) imaging of breast tissue: A numerical study of planar elliptical antennas applied to ultrawideband (UWB) imaging of breast tissue LAP LAMBERT Academic Publishing

Carr K L 1989 Microwave Radiometry: Its Importance to the Detection of Cancer *IEEE Trans. Microwave Theory and Tech.* **37** 1862–1869

Conway J J, King L R, Belman A B and T Thorson J 1972 Detection of vesicoureteral reflux with radionuclide cystography *The American Journal of Roentgenology* **115** 720–727

de Gonzáles A B and Darby S 2004 Risk of cancer from diagnostic x-rays: estimates for the UK and 14 other countries *Lancet* **363** 345–351

Dietsch A, Camart J C, Sozanski J P, Prevost B, Mauroy B and Chive M 2000 Microwave thermochemotherapy in the treatment of the bladder carcinoma - electromagnetic and dielectric studies-clinical protocol *IEEE Transaction Biomedical Engineering* **47** 633–641

Enander B and Larson G 1974 Microwave radiometric measurements of the temperature inside a body *Electronics Letters* **10** 317–317

Gabriel C, Gabriely S and Corthout E 1996 The dielectric properties of biological tissues: I. literature survey *Phys. Med. Biol* **41** 2231 – 2249

Gray H 1942 Anatomy of the Human Body PHILADELPHIA: LEA & FEBIGER, twentieth edition

Guyton A and Hall J 2000 Textbook of Medical Physiology W.B. Saunders Company, The Curtis Center, Independence Squares West, Philadelphia, Pensylvania 19106, USA tenth edition

Hand J, Leeuwen G V, Mizushina S, de Kamer J V, Maruyama K, Sugiura T, Azzopardi D and Edwards A 2001 Monitoring of deep brain temperature in infants using multi-frequency microwave radiometry and thermal modelling *Phys. Med. Biol.* **46** 1885–1903

Higashi T and Ishihara K 1990 Measurement of the complex relative permittivity frequency characteristics of the body using pulse-reflection *Electronics and Communications in Japan* **73** 841–849

Hiraoka M, Tsukahara H, Tsuchida S, Hori C and Sudo M 1995 Ultrasonic evaluation of bladder volume in young children *Pediatric Nephrology* **9** 351–353

Jacobsen S and Birkelund Y 2010 Improved resolution and reduced clutter in ultra-wideband microwave imaging using cross-correlated back projection: Experimental and numerical results *International Journal of Biomedical Imaging* **vol. 2010** 10

Jacobsen S and Klemetsen Ø 2008 Improved detectability in medical microwave radiothermometers as obtained by active antennas *IEEE Transactions on Biomedical Engineering* **55** 2778–2785

Jacobsen S and Stauffer P 2003 Nonparametric 1-D temperature restoration in lossy media using tikonov regularization in sparse radiometry data *IEEE Transactions on Biomedical Engineering* **50** 178–188

Jacobsen S and Stauffer P 2007 Can we settle with single-band radiometric temperature monitoring during hyperthermia treatment of chestwall recurrence of breast cancer using a dual-mode transceiving applicator? *Physics in Medicine and Biology* **52** 911–928

Jiang L, Zhan W and and M H L 2011 Modeling static and dynamic thermography of the human breast under elastic deformation *Physics in Medicine and Biology* **56** 187–202

Kennedy D A, Lee T and Seely D 2009 A comparative review of thermography as a breast cancer screening technique *Integrative Cancer Therapies* **8** 9–16

Kerr Y H, Waldteufel P, Wigneron J P, Martinuzzi J M, Font J and Berger M 2001 Soil moisture retrieval from space: The soil moisture and ocean salinity (smos) mission *IEEE T. Geosci. Remote* **39** 1729–1735

Klemetsen Ø, Birkelund Y, Jacobsen S K, Maccarini P F and Stauffer P R 2011 Design of medical radiometer front-end for improved performance *Progress In Electromagnetics Research B* **27** 289–306

Land D 1983 Radiometer receivers for microwave thermography *Microwave Journal* **19** 1040–1042

Lazebnik M, Okoniewski M, Booske J H and Hagness S C 2007 Highly accurate debye models for normal and malignant breast tissue dielectric properties at microwave frequencies *IEEE Microw. Wireless Comp. Lett.* **17** 822–824

Leroy Y, Bocquet B and Mamouni A 1998 Non-invasive microwave radiometry thermometry *Physiol. Meas.* **19** 127–148

Leroy Y, Mamouni A, Velde J V D, Bocquet B and Dujardin B 1987 Microwave Radiometry For Non-invasive Thermometry *Automedica* **8** 181–202

Meissner T and Wentz F J 2004 The complex dielectric constant of pure and sea water from microwave satellite observations *IEEE Transactions on Geoscience and Remote Sensing* **42** 1836–1849

Mizushina S, Ohba H, Abe K, Mizoshira S and Sugiura T 1995 Recent Trends in Medical Microwave Radiometry *IEICE Trans. Commun.* **E78-B** 789–798

Netter F H 1997 Atlas of Human Anatomy ICON Learning System

Paltiel H J, Rupich R C and Kiruluta H G 1992 Enhanced detection of vesicoureteral reflux in infants and children with use of cyclic voiding cystourethrography *Radiology* **184** 753–755

Pozar D M 2004 Microwave Engineering John Wiley and Sons 3rd edition

Reeves R, Anson A and Landen D 1975 Manual of Remote Sensing volume I American Society of Photogrammetry,Virginia,USA., 105 N, Virginia Ave. Falls Church, Va 22046 first edition

Semer N B and Adler-Lavan M 2001 Practical Plastic Surgery for Nonsurgeons HANLEY & BELFUS, INC. Medical Publishers 210 S. 13th Street Philadelphia, PA 19107

Sherwood L 2001 Human Physiology From Cells to Systems Brooks/Cole Thomson Learning fourth edition

Shiffman M A, editor 2010 Autologous Fat Transfer Art, Science, and Clinical Practice Springer Heidelberg Dordrecht London New York

Snow B W, Arunachalam K, De Luca V, Klemetsen Ø, Birkelund Y, Stauffer P R and Maccarini P F 2011 Non-invasive vesicoureteral reflux detection: Heating risk studies for a new device *Journal of Pedriatric Urology* **Accepted May 2011**

Snow B W and Taylor M B 2010 Non-invasive vesicoureteral reflux imaging *Journal of Pediatric Urology* **6** 543–549

Stauffer P R, Maccarini P, Arunachalam K, Craciunescu O, Diederich C, Juang T, Rossetto F, Schlorff J, Milligan A, Hsu J, Sneed P and Vujaskovic Z 2010 Conformal microwave array (cma) applicators for hyperthermia of diffuse chest wall recurrence *International Journal of Hyperthermia* **26** 686–698

Stec B, Dobrowolski A and Susek W 2004 Multifrequency Microwave Thermograph for Biomedical Applications *IEEE Trans. Biomedical Eng.* **51** 548–551

Ulaby F, Moore R and Fung A 1981 Microwave Remote Sensing volume I Microwave Remote Sensing Fundamentals and Radiometry Artec House, 685 Canton Street, Norwood, MA 02062, USA first edition

Zheng H and Smith C E 1991 Permittivity measurements using a short open-ended coaxial line probe *IEEE Microwave and Guided Wave Letters* **1** 337–339